Remarkable efficiency of Ni catalysts supported on hydrothermally synthesized CeO_2 nanorods for the low-temperature CO_2 hydrogenation to methane

Georgios Varvoutis[1,2], Maria Lykaki[3], Sofia Stefa[3], Eleni Papista[1], Sónia A.C. Carabineiro[4,5], Georgios E. Marnellos[1,2], Michalis Konsolakis[3]*

[1] Department of Mechanical Engineering, University of Western Macedonia, GR-50100, Kozani, Greece
[2] Chemical Process & Energy Resources Institute, Centre for Research & Technology Hellas, GR-57001, Thessaloniki, Greece
[3] School of Production Engineering and Management, Technical University of Crete, GR-73100, Chania, Greece
[4] Laboratory of Catalysis and Materials (LCM), Associate Laboratory LSRE-LCM, Faculty of Engineering, University of Porto, 4200-465 Porto, Portugal
[5] LAQV-REQUIMTE, Department of Chemistry, NOVA School of Science and Technology, Universidade NOVA de Lisboa, 2829-516 Caparica, Portugal

***** Correspondence: mkonsol@pem.tuc.gr; Tel.: +30-28210-37682; Web: http://ieesl.tuc.gr/

ABSTRACT

Nickel particles impregnated on hydrothermally synthesized ceria nanorods (CeO_2-NR) were found to be highly active and stable for CO_2 methanation at atmospheric pressure. A CO_2-to-CH_4 yield up to 92% was achieved at temperatures as low as 300 ^oC. The impact of various parameters, involving the H_2:CO_2 ratio, time-on-stream and space velocity was explored in conjunction with a thermodynamic analysis. The superior methanation performance of as-synthesized Ni/CeO_2-NR was demonstrated through a comparison with: a) corresponding CeO_2 and Ni/CeO_2 commercial samples, ii) various M/CeO_2-NR samples, emphasizing on the middle-late 3d metals (M = Cu, Co, Fe), and iii) state-of-the-art literature catalysts. The results revealed that a unique combination of Ni particles with ceria nanorods is required towards boosting the reducibility and in turn the methanation efficiency of Ni/CeO_2 catalysts.

Keywords: CO_2 methanation; Ni catalyst; ceria nanorods

Highlights:

- CeO_2 nanorods were synthesized by a facile hydrothermal method
- Ni/CeO_2-nanorods exhibited excellent CO_2 methanation performance
- A CO_2-to-CH_4 yield up to 92% was obtained at 300 ^oC
- Enhanced reducibility of Ni/CeO_2 linked to nickel-ceria nanorods interactions
- Superior methanation performance compared to most state-of-the-art Ni-based catalysts

1. Introduction

Methanation of carbon dioxide is one of the main pathways for effectively mitigating CO_2 emissions along with producing a valuable chemical like CH_4. However, the presence of a catalyst is necessary in order to overcome the problem of activating CO_2 molecule and enhance the reaction kinetics [1]. Despite the high methanation activity and stability of noble-metal catalysts [2,3], their high cost and scarcity render them financially impractical. However, nickel is widely considered as the optimum metallic phase, combining low cost and high methane yields [4]. The development of Ni-based catalysts for low-temperature CO_2 methanation is essential in order to reduce the overall cost of the process and to avoid catalyst deactivation through phenomena generally occurring at higher temperatures, such as sintering of Ni particles or carbon deposition [5].

Regarding the supporting materials, ceria has attracted considerable attention over the past years, due to its excellent redox properties, oxygen storage capacity and remarkable thermal stability [6]. Notably, by adjusting the morphology of ceria particles in the nanoscale (e.g., nanocubes, nanorods), distinct crystal facets can be exposed, with implications in the aforementioned intrinsic characteristics but also in metal-support interactions [7,8]. In this regard, we recently showed by means of *in situ* and *ex situ* techniques that among ceria nanoparticles of different morphology, ceria nanorods preferentially exposing the {110} and {111} planes, exhibited the optimum redox properties in terms of loosely-bound oxygen species and oxygen mobility [9]. Moreover, it was reported that catalysts based on ceria nanorods were highly active in CO oxidation [9], water-gas shift [10], NO reduction by CO [11], steam reforming of methanol [12] and CO_2 reforming of methane [13].

Thus, taking into account the key role of support reducibility on the CO_2 methanation process [14], we prepared and catalytically evaluated composites of nickel supported on ceria nanorods, Ni/CeO_2-NR, in the CO_2 methanation reaction. Herein, we highlight the excellent low-temperature methanation activity of Ni/CeO_2-NR; CO_2 conversion and CH_4 selectivity reached thermodynamic equilibrium values at temperatures as low as 300 ^oC. Moreover, the sample demonstrated excellent stability in short-term (24 h) stability experiments. The superiority of Ni/CeO_2-NR was further verified through a comparison with the commercial CeO_2 and Ni/CeO_2 samples, various CeO_2-NR based transition metals, and state-of-the-art Ni-based catalysts.

2. Experimental

2.1. Catalysts preparation and characterization

Bare ceria nanoparticles with a rod-like morphology were synthesized by the hydrothermal method, as described in detail in our previous work [13]. The bare ceria nanorod sample is designated as CeO_2-NR. Ni/CeO_2-NR catalysts were synthesized by the wet impregnation method, in order to obtain a nickel loading of ca. 8 wt.%, which corresponds to a Ni/(Ni+Ce) atomic ratio of 0.2. The sample was dried at 90 ^oC for 12 h and finally calcined at 500 ^oC for 2 h under air flow (heating ramp 5 ^oC/min). Various transition metal catalysts (M/CeO_2-NR, M=Cu, Co, Fe), with the same M/(M+Ce) atomic ratio, were synthesized following exactly the same preparation procedure. For comparison purposes, commercial ceria (Aldrich, 99.9%, <5 micron) was used (CeO_2-C). Ni/CeO_2-C sample was prepared following the aforementioned procedure with only one exception: CeO_2-C instead of CeO_2-NR was used. The as-prepared samples were characterized by N_2 adsorption-desorption at -196 ^oC, X-ray powder diffraction (XRD), X-ray Photoelectron Spectroscopy (XPS), temperature-programmed reduction with hydrogen (H_2-TPR) and transmission electron microscopy (TEM), as described in more details elsewhere [9,15]. Indicative samples were further characterized after a reduction pre-treatment (100% v/v H_2 at 400 ^oC for 2 h).

2.2. Catalytic evaluation studies

The apparatus and operating conditions of the catalytic evaluation studies were similar to the ones employed in our previous work [22]. Briefly, the catalyst bed consisted of a mixture of 200 mg of

catalyst diluted with 200 mg of inert SiO_2. Prior to experiments, catalysts were reduced *in situ* at 400 ^oC for 1 h under pure H_2 flow (40 mL/min), followed by flushing with He. All experiments were conducted at atmospheric pressure and in the temperature range of 200 - 400 ^oC at intervals of 15-20 ^oC and a heating rate of 1 ^oC/min. The total flow rate of the feed gas was 100 mL/min, corresponding to a weight hourly space velocity (WHSV) of 30,000 $mL \cdot g^{-1} \cdot h^{-1}$. Gas feed constituted of H_2/CO_2 mixtures at different molar ratios (1-9).

The thermodynamic equilibrium calculations were derived from the mathematical model RGibbs in Aspen Plus software, which minimizes the Gibbs free energy of a system. Only CH_4 and CO were detected as carbonaceous products in the reactor outlet stream of the experiments. Conversion of CO_2 (X_{CO2}) and selectivity to CH_4 and CO (S_i) were calculated by the following equations (Eqs 2-4):

$$\% X_{CO_2} = \frac{([CO_2]_{in} \cdot F_{in}) - ([CO_2]_{out} \cdot F_{out})}{[CO_2]_{in} \cdot F_{in}} \cdot 100 \quad (2)$$

$$\% S_{CO} = \frac{[CO]_{out}}{[CO]_{out} + [CH_4]_{out}} \cdot 100 \quad (3)$$

$$\% S_{CH_4} = \frac{[CH_4]_{out}}{[CO]_{out} + [CH_4]_{out}} \cdot 100 \quad (4)$$

where $[i]_{in}$ and $[i]_{out}$ represent the concentrations of reactant ($i = CO_2$) or products ($i = CO, CH_4$) at the inlet and outlet of the reactor, respectively. F_{in} and F_{out} are the total flow rates at the inlet and outlet of the reactor, respectively.

3. Results and discussion

3.1. Catalysts characterization

The distinct rod-like morphology of ceria nanoparticles was verified by TEM (**Figure 1a**). The rods length varies between 25 and 200 nm. Ni incorporation into the CeO_2-NR does not alter the morphology of bare ceria.

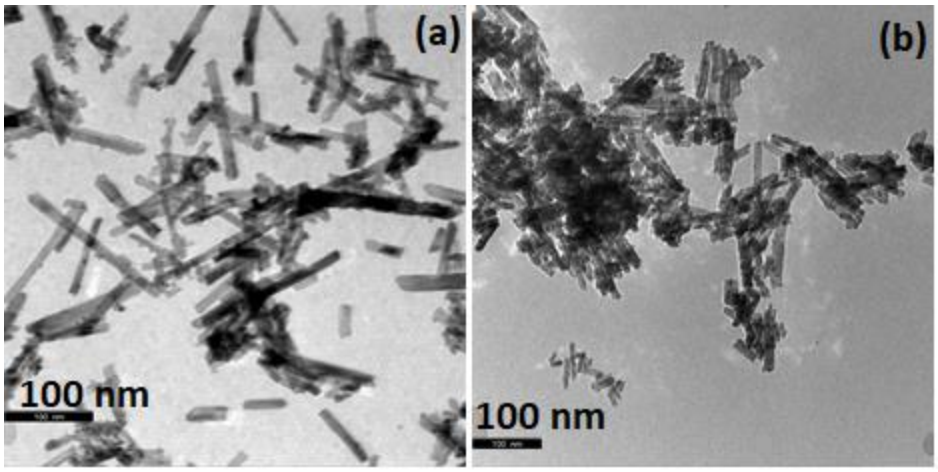

Figure 1. TEM images of CeO_2-NR (a) and Ni/CeO_2-NR (b) samples.

Bare CeO2-NR shows a BET surface area of 79 m^2/g, which is slightly decreased by metal incorporation to ceria carrier. The crystallite size of CeO_2-NR is 15 nm and it remained mostly unaffected by metal incorporation.

Table 1 summarizes the main physicochemical and redox properties of the samples. XRD diffractograms of the calcined samples (not shown) demonstrated the existence of CuO, Co_3O_4, NiO and Fe_2O_3 for Cu-, Co-, Ni- and Fe/CeO_2 samples, respectively, with no peaks associated with other crystal phases, except ceria. Crystallite sizes of ceria and the corresponding metal oxide phases were calculated and are also presented in **Table 1**. Bare CeO_2-NR shows a BET surface area of 79 m^2/g, which is slightly decreased by metal incorporation to ceria carrier. The crystallite size of CeO_2-NR is 15 nm and it remained mostly unaffected by metal incorporation.

Table 1. Physicochemical and redox properties of the as-prepared M/CeO_2-NR samples.

Sample	BET Analysis	XRD Analysis		H_2-TPR Analysis	
	S_{BET} (m^2/g)	Average crystallite diameter, D_{XRD} (nm)		H_2 consumption (mmol $H_2 \cdot g^{-1}$)[a]	Theoretical H_2 (mmol $H_2 \cdot g^{-1}$)[b]
		CeO_2	M_xO_y		
CeO_2-NR	79	15	-	0.59	-
Ni/CeO_2-NR	72	14	23	1.82	1.34
Fe/CeO_2-NR	69	10	7	1.60	2.02
Co/CeO_2-NR[c]	72	14	16	2.37	1.76
Cu/CeO_2-NR[c]	75	12	43	1.80	1.34

[a] *Estimated by the quantification of H_2 uptake in the range 100-700 °C of the H_2-TPR profiles.*

[b] *Calculated as the amount of H_2 required for the complete reduction of fully oxidized M_xO_y to M^0.*
[c] *Reproduced from Ref.* [15].

In **Erro! Autorreferência de marcador inválida.** the H_2-TPR profiles of CeO_2-NR and M/CeO_2-NR samples are depicted. Bare ceria exhibits two peaks at high temperatures (589 and 809 °C), attributed to the reduction of surface and bulk oxygen species of CeO_2, respectively [17]. The facilitation of the ceria surface oxygen reduction in the presence of a metal phase results in overlapping bands in the low-temperature (LT) range of the TPR profiles of all M/CeO_2 samples. Thus, the LT reduction peaks of M/CeO_2 samples can be attributed to the consecutive reduction of surface ceria oxygen and M_xO_y species, with the effect being more prominent in the case of Cu/CeO_2-NR. With the exception of Fe/CeO_2-NR, all samples exhibit peaks at much lower temperatures than bare ceria support and are fully reduced at temperatures lower than ca. 500 °C. Also, hydrogen consumption exceeded the theoretical amount (**Table 1**), conducive to the fact that reducibility of ceria nanorods is substantially enhanced upon addition of metallic phases, due to metal-support synergistic interactions [18].

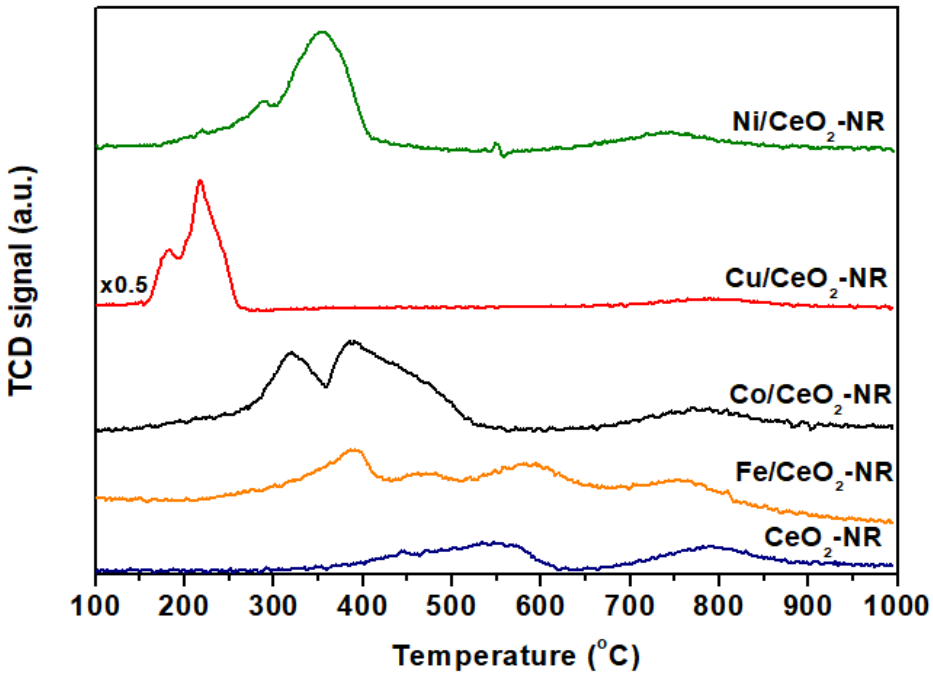

Figure 2. H_2-TPR results of the as-prepared CeO_2-NR and M/CeO_2-NR samples.

Figure 3a depicts the Ce 3d XPS spectra of the as-prepared (Ni/CeO_2-NR) and reduced (Ni/CeO_2-NR-red) nickel-ceria samples. In particular, the Ce 3d core level spectra (**Figure 3a**) are deconvoluted into three pairs of spin-orbit doublets (u, v; u", v"; and u"', v"') corresponding to Ce^{4+} and into two peaks (u' and v') of Ce^{3+} [19]. The assignment of these characteristic peaks has been described in a previous work [9]. Interestingly, the reduced sample exhibits double the amount of Ce^{3+} species (30.4%), as compared to the as-prepared sample (14.2%), implying the facile reduction of ceria nanorods under reducing conditions (H_2-pretreatment), as those prevail under reaction conditions. Moreover, the reduced Ni/CeO_2-NR samples exhibit the highest amount of Ce^{3+} species (30.4%) as compared to the corresponding Fe/CeO_2-NR (26.9%), Co/CeO_2-NR (29.9%) and Cu/CeO_2-NR (25.5%), implying the facile reduction of ceria nanorods in the presence of nickel. Similar results have been previously obtained over Ni/CeO_2 catalysts, attributed to the hydrogen spill-over effect; dissociation of molecular hydrogen on the metal surface results in highly mobile atomic hydrogen which reduces ceria adjacent to the metal [20]. Recently, it was shown by means of *in situ* studies that Ce^{3+} species play a key role on the reaction mechanism, as they facilitate the activation of the CO_2 molecules [21].

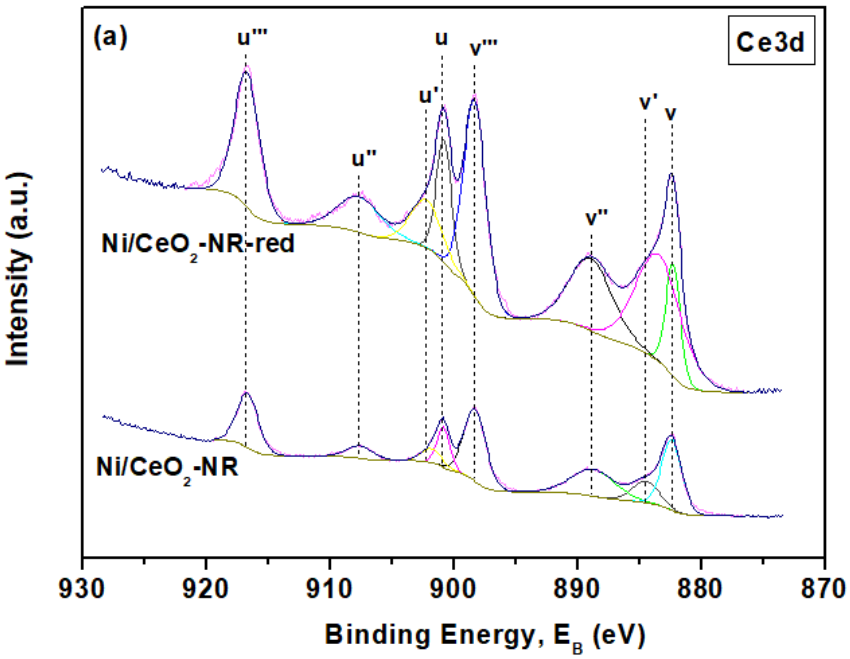

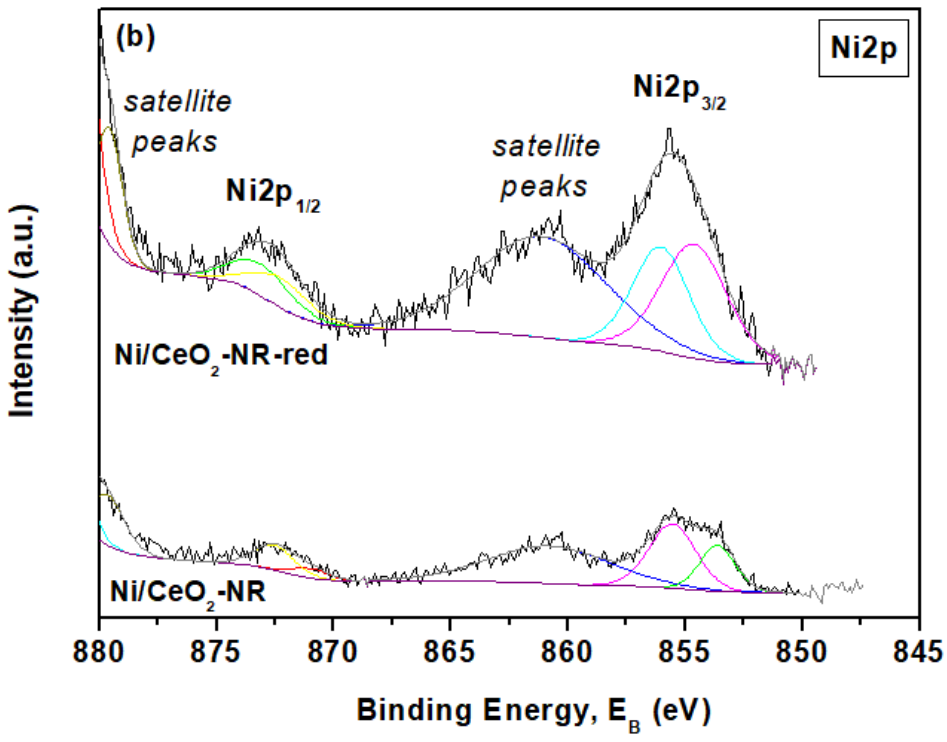

Figure 3. XPS spectra of Ce 3d (a) and Ni 2p (b) of the as-prepared and reduced Ni/CeO_2-NR samples.

In **Figure 3b**, the Ni 2p XPS spectra of the as-prepared and reduced Ni/CeO_2-NR samples are depicted. The samples exhibit two main peaks around 855.5 eV and 873 eV, which correspond to Ni $2p_{3/2}$ and Ni $2p_{1/2}$, respectively. The as-prepared sample exhibits multi-split peaks at 853.5 eV and 855.5 eV, along with a broad satellite peak at around 861 eV, which correspond to the characteristic Ni $2p_{3/2}$ of NiO and/or $Ni(OH)_2$ species [22–24]. In the reduced sample, the Ni $2p_{3/2}$ peak appears at a binding energy well above that of NiO, which is characteristic of $Ni(OH)_2$ species [25]. In particular, the peak at low binding energy (853.5 eV) can be ascribed to Ni^{2+} species in the octahedral configuration of NiO, the peak at higher binding energy (855.5 eV) can be attributed to defective or hydroxylated NiO, namely Ni^{2+} vacancy-induced Ni^{3+} ion or nickel hydroxides and oxyhydroxides, respectively, while the peak at the highest binding energy (~860.6 eV) corresponds to a shake-up process in the lattice of NiO [26]. In this point, it should be mentioned that due to the various possible sources of assigning the XPS peak at around 855.5 eV, more sophisticated characterization techniques should be applied [26].

3.2. Catalytic evaluation studies

In **Figure 4**, the CO_2 conversion (a) and selectivity to CH_4 (b) as a function of the reaction temperature are depicted for the as-prepared CeO_2-NR and M/CeO_2-NR samples. The superior methanation performance of Ni/CeO_2-NR is evident, offering a maximum CO_2 conversion of 92.1% at 300 ^oC having practically reached the equilibrium values. In terms of CO_2 conversion, the following order was recorded: Ni/CeO_2-NR > Co/CeO_2-NR > Cu/CeO_2-NR > Fe/CeO_2-NR > CeO_2-NR, demonstrating the beneficial effect of metal incorporation into the ceria nanorod support. Notably, the onset methanation temperature of the Ni catalyst is ca. 215 ^oC, whereas all the other samples were practically inert below ca. 270 ^oC. The as-prepared Ni catalyst is completely selective towards methane at all temperatures investigated.

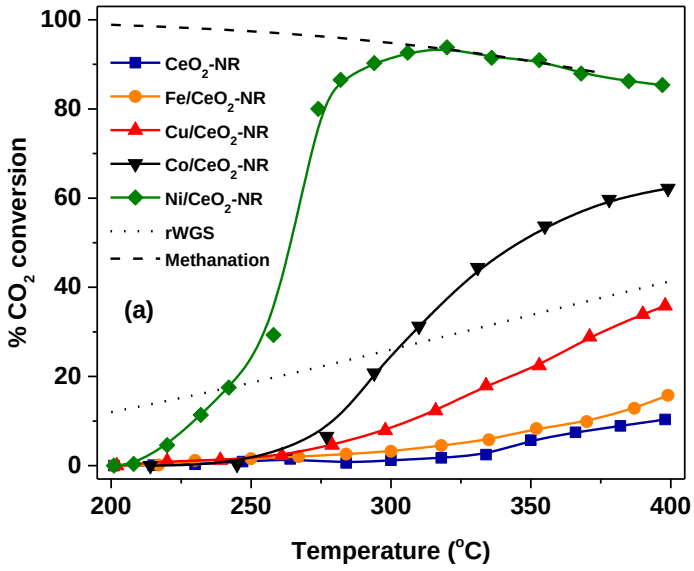

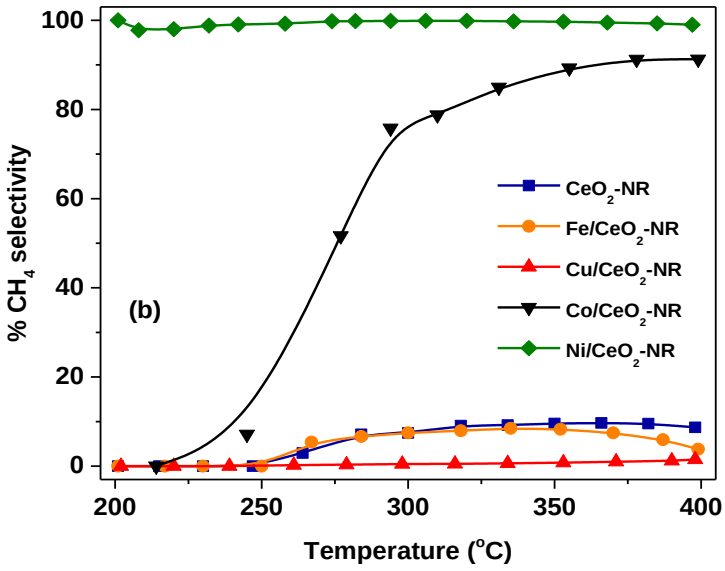

Figure 4. CO_2 conversion (a) and CH_4 selectivity (b) profiles for bare CeO_2-NR and M/CeO_2-NR samples. Reaction conditions: WHSV = 30,000 $mL \cdot g^{-1} \cdot h^{-1}$, H_2:CO_2 = 4:1, P = 1 atm.

To further demonstrate the superior performance of Ni/CeO_2-NR sample, a comparison with the corresponding commercial samples, CeO_2-C and Ni/CeO_2-C, is performed (**Figure 5**). Obviously, Ni/CeO_2-NR is far more active and selective towards CH_4 than Ni/CeO_2-C, indicating the key role of ceria nanostructure. CeO_2-C and Ni/CeO_2-C exhibit CH_4 selectivity of 20% and 63% at 300 °C, respectively, whereas the corresponding values for CeO_2-NR and Ni/CeO_2-NR are 8% and 99%. These results are conducive of the fact that the nickel phase is indispensable for the production of CH_4. Interestingly, although CeO_2-NR exhibits the worst performance in terms of CH_4 selectivity, its combination with Ni boosts the selectivity to values close to 100%.

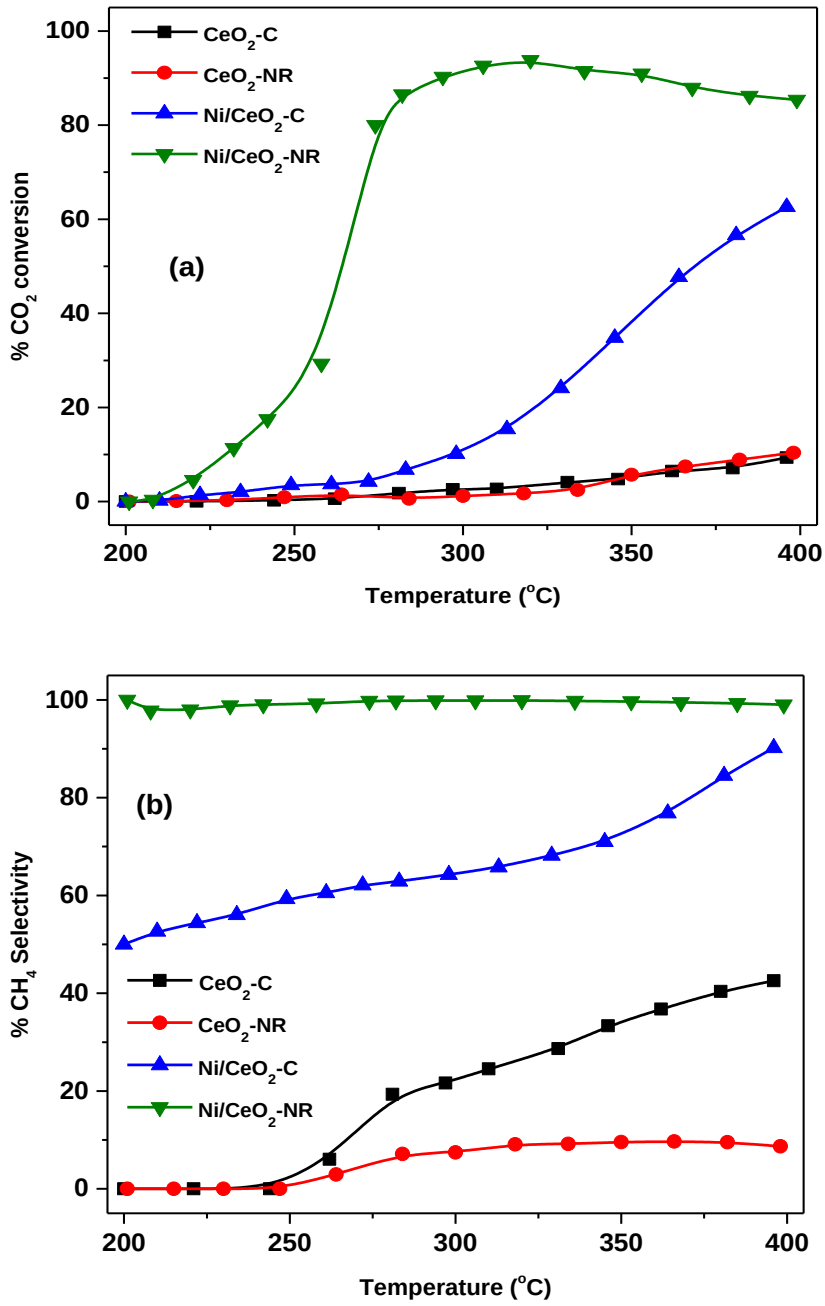

Figure 5. CO_2 conversion (a) and CH_4 selectivity (b) profiles for CeO_2-C, Ni/CeO_2-C, CeO_2-NR and Ni/CeO_2-NR samples. Reaction conditions: WHSV = 30,000 $mL \cdot g^{-1} \cdot h^{-1}$, H_2:CO_2 = 4:1, P = 1 atm.

The methanation performance of Ni/CeO_2-NR was also investigated under different reactant ratios (**Figure 6**). An increase in hydrogen concentration exerts a beneficial effect in CO_2 conversion, reaching the value of 99.5% at 300 °C and at a high H_2:CO_2 ratio of 9, in agreement to literature

[27]. Selectivity to methane was higher than 90% even under the sub-stoichiometric ratio of 1, further corroborating the excellent methanation performance of the sample.

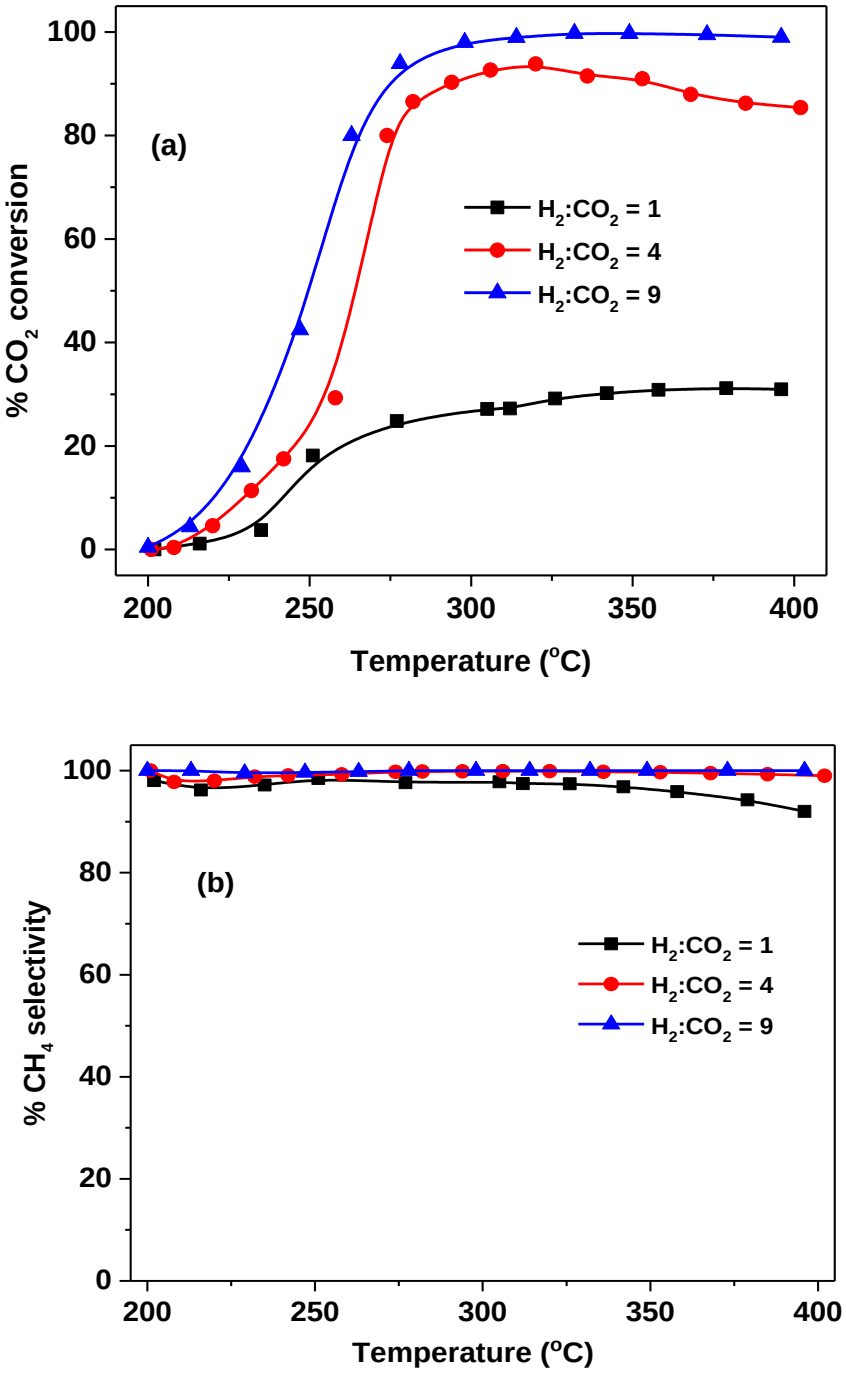

Figure 6. Effect of H_2:CO_2 ratio as a function of temperature on CO_2 conversion (a) and CH_4 selectivity (b) for Ni/CeO_2-NR. Reaction conditions: WHSV = 30,000 mL·g^{-1}·h^{-1}, P = 1 atm.

The effect of the weight hourly space velocity was next examined (

Figure 7). At 300 ^{o}C, CO_2 conversion reached values of 98.1, 90.8 and 83.2% for a WHSV of 30,000, 60,000 and 120,000 $mL \cdot g^{-1} \cdot h^{-1}$, respectively. Similar results have been reported elsewhere in the literature [28]. It should be also noted that regardless of the WHSV used, the selectivity to methane remains practically 100% (not shown). Moreover, a stable performance was recorded in short-term (24 h) stability tests at 350 ^{o}C, without any deterioration on activity/selectivity (not shown).

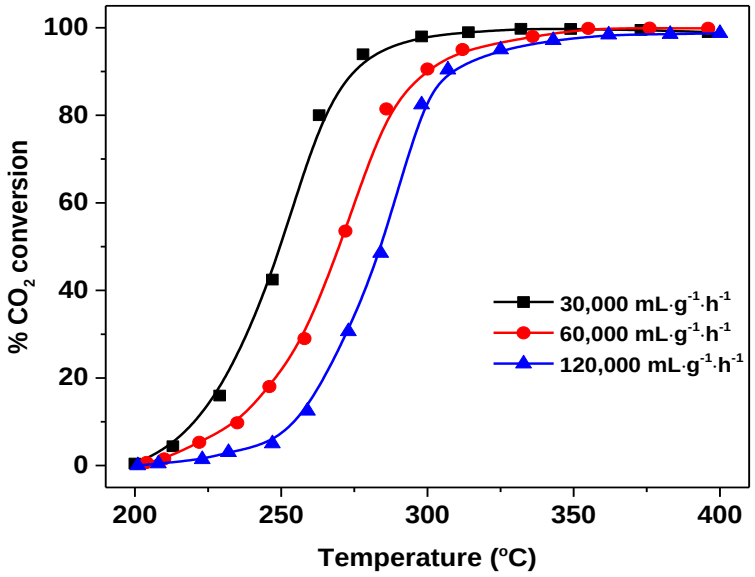

Figure 7. Effect of WHSV and reaction temperature on CO_2 conversion for Ni/CeO_2-NR. H_2:CO_2 = 9:1, P = 1 atm.

To further demonstrate the high methanation activity of the as-synthesized Ni/CeO_2-NR catalyst, its performance is compared to that of various state-of-the-art Ni-based catalysts for low-temperature CO_2 methanation reported in the literature (**Table**). The overall superiority of the as-prepared Ni/CeO_2-NR sample in terms of various parameters such as metal loading, space velocity, conversion/selectivity efficiency and low-temperature activation is evident. It is worth noticing that the achieved CO_2 conversion value of 92.1% at 300 ^{o}C is very close to the one predicted by thermodynamics (94.1%). Lastly, the superiority of Ni/CeO_2-NR samples can be further justified by comparison with the state-of-the-art ceria-based methanation catalysts, comprehensively summarized by Chang *et al.* [29].

Table 2. Comparison of the as-prepared Ni/CeO_2-NR sample with the state-of-the-art Ni-based catalysts for low-temperature CO_2 methanation. (H_2:CO_2 = 4:1, P = 1 atm).

Catalyst	T (ºC)	WHSV ($mL \cdot g^{-1} \cdot h^{-1}$)	Ni loading (wt.%)	X_{CO2}	S_{CH4}	Ref.
Ni/CeO_2-NR	*300*	*30,000*	*~8*	*92.1*	*99.8*	*This work*
Ni/CeO_2-NR	250	24,000	5	23.5	~100	[20]
$Ni/Ce_{0.72}Zr_{0.28}O_2$	350	43,000[1]	10	85.7	99.7	[28]
Ni-Al/CeO_2	250	2,400[1]	25.6	91	99	[30]
Ni/CeO_2	300	14,000	10	87.2	99	[31]
Sponge Ni (commercial)	300	*n/a*	> 92.5	87.5	> 95	[32]
Ni/CeO_2	340	45,000	*n/a*	91.1	100	[33]
Ni/CeO_2	300	10,000[1]	10	~90	~100	[34]
Ni/CeO_2[2]	340	22,000	10	91.1	100	[35]
Ni/ZrO_2	350	45,000	15	84.1	99.5	[36]
Ni/CeO_2-SGM	300	10,000	20	86.5	91.3	[37]

[1] *Space velocity is provided in units of h^{-1}*
[2] *H_2:CO_2 = 4.6*

The superior performance of Ni/CeO_2-NR could be attributed to the improved reducibility and oxygen exchange kinetics, offered mainly by ceria nanorods, as has been previously revealed [9]. This is in accordance with the abundance of reduced Ce^{3+} species, as shown by XPS and H_2-TPR analyses (see above). In particular, nickel can easily dissociate gaseous hydrogen into H adatoms onto the catalytic surface [38]. These $H_{(ad)}$ moieties can then migrate to ceria, hydrogenating the species formed upon CO_2 adsorption and thus a CH_4 molecule can be facilely produced and be desorbed as $CH_{4(g)}$ [4]. In view of these aspects, it was very recently shown by means of isotopic and *in situ* DRIFTS studies that the higher methanation activity of Ni/CeO_2 compared to Ni/Al_2O_3 catalysts can be mainly attributed to the peculiar nickel-ceria interactions and to the high oxygen mobility of ceria, which hinders the accumulation of water and carbon-containing species on the catalyst surface [39]. In a similar manner, the increased methanation activity of CeO_2-based samples has been ascribed to the high concentration of Ce^{3+} species, which led to higher formate coverage [4,20,21,40]. In view of this fact, the Ni/CeO_2 catalyst was found to be the most active for CO_2 methanation in comparison to other lanthanide-supported nickel catalysts due to the strong interaction between nickel and ceria, and the electronegativity of the reduced nickel species where

the hydrogen dissociation takes place [23]. Therefore, on the basis of the present preliminary studies, the superiority of Ni/CeO_2-NR could be attributed to the peculiar synergistic interactions between the nickel and ceria nanorods towards enhancing the reducibility (high population of Ce^{3+} species) and in turn the CO_2 methanation performance.

4. Conclusions

In the present work we reported on a highly efficient nickel catalyst supported on ceria nanorods for the low-temperature production of CH_4 through the CO_2 hydrogenation process. The as-prepared catalyst showed excellent methanation performance at temperatures as low as ca. 300 ^oC, being superior to most of the state-of-the-art nickel-based catalysts. The effect of ceria nanorod morphology was crucial, since a nickel catalyst supported on commercially available CeO_2 exhibited far inferior performance. The combination of Ni with ceria nanoparticles of rod-like morphology is necessary towards the formation of highly active and selective Ni/CeO_2 for low temperature methanation process. Encouraged by these promising results, further work is currently being conducted in order to elucidate the role of the support nanostructure and the underlying mechanism of the reaction.

Author contributions

M.L., S.S., S.A.C.C and E.P. contributed to materials synthesis, characterizations and catalytic evaluation studies; M.K. contributed to the conception, design and results interpretation; M.K. and G.E.M. validated the results and administered the project. G.V. and M.L. wrote the original draft. Finally, M.K. reviewed, edited and submitted the manuscript in the final form. All authors contributed to the discussion, read and approved the final version of the manuscript.

Acknowledgments

This research has been co-financed by the European Union and Greek national funds through the Operational Program Competitiveness, Entrepreneurship and Innovation, under the call RESEARCH - CREATE - INNOVATE (project code: T1EDK-00094). This work was also financially supported by Investigador FCT program (IF/01381/2013/CP1160/CT0007), base

funding UIDB/50020/2020 of the Associate Laboratory LSRE-LCM, funded by national funds through FCT/MCTES (PIDDAC) and Associate Laboratory for Green Chemistry – LAQV, financed by national funds from FCT/MCTES (UIDB/50006/2020). Authors are grateful to Dr. Carlos Sá (CEMUP) and Prof. Pedro Tavares (UTAD) for assistance with XPS and TEM measurements, respectively.

References

[1] M. Younas, L. Loong Kong, M.J.K. Bashir, H. Nadeem, A. Shehzad, S. Sethupathi, Recent Advancements, Fundamental Challenges, and Opportunities in Catalytic Methanation of CO_2, Energy Fuels. 30 (2016) 8815–8831. https://doi.org/10.1021/acs.energyfuels.6b01723.

[2] C. Swalus, M. Jacquemin, C. Poleunis, P. Bertrand, P. Ruiz, CO_2 methanation on Rh/γ-Al_2O_3 catalyst at low temperature: "*In situ*" supply of hydrogen by Ni/activated carbon catalyst, Appl. Catal. B Environ. 125 (2012) 41–50. https://doi.org/10.1016/j.apcatb.2012.05.019.

[3] P.J. Lunde, F.L. Kester, Carbon Dioxide Methanation on a Ruthenium Catalyst, Ind. Eng. Chem. Process Des. Dev. 13 (1974) 27–33. https://doi.org/10.1021/i260049a005.

[4] J. Lin, C. Ma, Q. Wang, Y. Xu, G. Ma, J. Wang, H. Wang, C. Dong, C. Zhang, M. Ding, Enhanced low-temperature performance of CO_2 methanation over mesoporous Ni/Al_2O_3-ZrO_2 catalysts, Appl. Catal. B Environ. 243 (2019) 262–272. https://doi.org/10.1016/j.apcatb.2018.10.059.

[5] X. Guo, A. Traitangwong, M. Hu, C. Zuo, V. Meeyoo, Z. Peng, C. Li, Carbon Dioxide Methanation over Nickel-Based Catalysts Supported on Various Mesoporous Material, Energy Fuels. 32 (2018) 3681–3689. https://doi.org/10.1021/acs.energyfuels.7b03826.

[6] M. Capdevila-Cortada, G. Vilé, D. Teschner, J. Pérez-Ramírez, N. López, Reactivity descriptors for ceria in catalysis, Appl. Catal. B Environ. 197 (2016) 299–312. https://doi.org/10.1016/j.apcatb.2016.02.035.

[7] M. Konsolakis, The role of Copper–Ceria interactions in catalysis science: Recent

theoretical and experimental advances, Appl. Catal. B Environ. 198 (2016) 49–66. https://doi.org/10.1016/j.apcatb.2016.05.037.

[8] C. Sun, H. Li, L. Chen, Nanostructured ceria-based materials: synthesis, properties, and applications, Energy Environ. Sci. 5 (2012) 8475–8505. https://doi.org/10.1039/c2ee22310d.

[9] M. Lykaki, E. Pachatouridou, S.A.C. Carabineiro, E. Iliopoulou, C. Andriopoulou, N. Kallithrakas-Kontos, S. Boghosian, M. Konsolakis, Ceria nanoparticles shape effects on the structural defects and surface chemistry: Implications in CO oxidation by Cu/CeO_2 catalysts, Appl. Catal. B Environ. 230 (2018) 18–28. https://doi.org/10.1016/j.apcatb.2018.02.035.

[10] R. Si, M. Flytzani-Stephanopoulos, Shape and Crystal-Plane Effects of Nanoscale Ceria on the Activity of $Au-CeO_2$ Catalysts for the Water-Gas Shift Reaction, Angew. Chem. Int. Ed. 47 (2008) 2884–2887. https://doi.org/10.1002/anie.200705828.

[11] L. Liu, Z. Yao, Y. Deng, F. Gao, B. Liu, L. Dong, Morphology and Crystal-Plane Effects of Nanoscale Ceria on the Activity of CuO/CeO_2 for NO Reduction by CO, ChemCatChem. 3 (2011) 978–989. https://doi.org/10.1002/cctc.201000320.

[12] N. Yi, R. Si, H. Saltsburg, M. Flytzani-Stephanopoulos, Steam reforming of methanol over ceria and gold-ceria nanoshapes, Appl. Catal. B Environ. 95 (2010) 87–92. https://doi.org/10.1016/j.apcatb.2009.12.012.

[13] X. Du, D. Zhang, L. Shi, R. Gao, J. Zhang, Morphology Dependence of Catalytic Properties of Ni/CeO_2 Nanostructures for Carbon Dioxide Reforming of Methane, J. Phys. Chem. C. 116 (2012) 10009–10016. https://doi.org/10.1021/jp300543r.

[14] J.A.H. Dreyer, P. Li, L. Zhang, G.K. Beh, R. Zhang, P.H.-L. Sit, W.Y. Teoh, Influence of the oxide support reducibility on the CO_2 methanation over Ru-based catalysts, Appl. Catal. B Environ. 219 (2017) 715–726. https://doi.org/10.1016/j.apcatb.2017.08.011.

[15] M. Konsolakis, M. Lykaki, S. Stefa, S.A.C. Carabineiro, G. Varvoutis, E. Papista, G.E. Marnellos, CO_2 Hydrogenation over Nanoceria-Supported Transition Metal Catalysts: Role of Ceria Morphology (Nanorods versus Nanocubes) and Active Phase Nature (Co versus

Cu), Nanomaterials. 9 (2019) 1739. https://doi.org/10.3390/nano9121739.

[16] T.A. Le, T.W. Kim, S.H. Lee, E.D. Park, Effects of Na content in Na/Ni/SiO_2 and Na/Ni/CeO_2 catalysts for CO and CO_2 methanation, Catal. Today. 303 (2018) 159–167. https://doi.org/10.1016/j.cattod.2017.09.031.

[17] T. Désaunay, G. Bonura, V. Chiodo, S. Freni, J.-P. Couzinié, J. Bourgon, A. Ringuedé, F. Labat, C. Adamo, M. Cassir, Surface-dependent oxidation of H_2 on CeO_2 surfaces, J. Catal. 297 (2013) 193–201. https://doi.org/10.1016/j.jcat.2012.10.011.

[18] M. Konsolakis, S.A.C. Carabineiro, E. Papista, G.E. Marnellos, P.B. Tavares, J. Agostinho Moreira, Y. Romaguera-Barcelay, J.L. Figueiredo, Effect of preparation method on the solid state properties and the deN_2O performance of CuO–CeO_2 oxides, Catal. Sci. Technol. 5 (2015) 3714–3727. https://doi.org/10.1039/C5CY00343A.

[19] W. Zou, C. Ge, M. Lu, S. Wu, Y. Wang, J. Sun, Y. Pu, C. Tang, F. Gao, L. Dong, Engineering the NiO/CeO_2 interface to enhance the catalytic performance for CO oxidation, RSC Adv. 5 (2015) 98335–98343. https://doi.org/10.1039/c5ra20466f.

[20] Z. Bian, Y.M. Chan, Y. Yu, S. Kawi, Morphology dependence of catalytic properties of Ni/CeO_2 for CO_2 methanation: A kinetic and mechanism study, Catal. Today. (2018) Article in press. https://doi.org/10.1016/j.cattod.2018.04.067.

[21] N.M. Martin, F. Hemmingsson, A. Schaefer, M. Ek, L.R. Merte, U. Hejral, J. Gustafson, M. Skoglundh, A.-C. Dippel, O. Gutowski, M. Bauer, P.-A. Carlsson, Structure-function relationship for CO_2 methanation over ceria supported Rh and Ni catalysts under atmospheric pressure conditions, Catal. Sci. Technol. 9 (2019) 1644–1653. https://doi.org/10.1039/c8cy02097c.

[22] J.F. Moulder, W.F. Stickle, P.E. Sobol, K.D. Bomben, Handbook of X-ray photoelectron spectroscopy (XPS), Perkin-Elmer Corporation, Eden Prairie, Minnesota, USA, 1992.

[23] V. Alcalde-Santiago, A. Davó-Quiñonero, D. Lozano-Castelló, A. Quindimil, U. De-La-Torre, B. Pereda-Ayo, J.A. González-Marcos, J.R. González-Velasco, A. Bueno-López, Ni/LnO_x Catalysts (Ln=La, Ce or Pr) for CO_2 Methanation, ChemCatChem. 11 (2019) 810–819. https://doi.org/10.1002/cctc.201801585.

[24] H. Li, H. Li, W.-L. Dai, W. Wang, Z. Fang, J.-F. Deng, XPS studies on surface electronic characteristics of Ni-B and Ni-P amorphous alloy and its correlation to their catalytic properties, Appl. Surf. Sci. 152 (1999) 25–34. https://doi.org/10.1016/S0169-4332(99)00294-9.

[25] M.J. Muñoz-Batista, L. Andrini, F.G. Requejo, M.N. Gómez-Cerezo, M. Fernández-García, A. Kubacka, Sunlight active g-C_3N_4-based M^{n+} (M=Cu, Ni, Zn, Mn) – promoted catalysts: Sharing of nitrogen atoms as a door for optimizing photo-activity, Mol. Catal. 484 (2020) 110725. https://doi.org/10.1016/j.mcat.2019.110725.

[26] J.R. Manders, S.-W. Tsang, M.J. Hartel, T.-H. Lai, S. Chen, C.M. Amb, J.R. Reynolds, F. So, Solution-Processed Nickel Oxide Hole Transport Layers in High Efficiency Polymer Photovoltaic Cells, Adv. Funct. Mater. 23 (2013) 2993–3001. https://doi.org/https://doi.org/10.1002/adfm.201202269.

[27] A. Swapnesh, V.C. Srivastava, I.D. Mall, Comparative Study on Thermodynamic Analysis of CO_2 Utilization Reactions, Chem. Eng. Technol. 37 (2014) 1765–1777. https://doi.org/10.1002/ceat.201400157.

[28] F. Ocampo, B. Louis, A.-C. Roger, Methanation of carbon dioxide over nickel-based $Ce_{0.72}Zr_{0.28}O_2$ mixed oxide catalysts prepared by sol-gel method, Appl. Catal. A Gen. 369 (2009) 90–96. https://doi.org/10.1016/j.apcata.2009.09.005.

[29] K. Chang, H. Zhang, M.-j. Cheng, Q. Lu, Application of Ceria in CO_2 Conversion Catalysis, ACS Catal. 10 (2020) 613-631. https://doi.org/10.1021/acscatal.9b03935.

[30] X. Guo, H. He, A. Traitangwong, M. Gong, V. Meeyoo, P. Li, C. Li, Z. Peng, S. Zhang, Ceria imparts superior low temperature activity to nickel catalysts for CO_2 methanation, Catal. Sci. Technol. 9 (2019) 5636–5650. https://doi.org/10.1039/c9cy01186b.

[31] C. Fukuhara, K. Hayakawa, Y. Suzuki, W. Kawasaki, R. Watanabe, A novel nickel-based structured catalyst for CO_2 methanation: A honeycomb-type Ni/CeO_2 catalyst to transform greenhouse gas into useful resources, Appl. Catal. A Gen. 532 (2017) 12–18. https://doi.org/10.1016/j.apcata.2016.11.036.

[32] S. Tada, S. Ikeda, N. Shimoda, T. Honma, M. Takahashi, A. Nariyuki, S. Satokawa, Sponge

Ni catalyst with high activity in CO_2 methanation, Int. J. Hydrogen Energy. 42 (2017) 30126–30134. https://doi.org/10.1016/j.ijhydene.2017.10.138.

[33] G. Zhou, H. Liu, K. Cui, H. Xie, Z. Jiao, G. Zhang, K. Xiong, X. Zheng, Methanation of carbon dioxide over Ni/CeO_2 catalysts: Effects of support CeO_2 structure, Int. J. Hydrogen Energy. 42 (2017) 16108–16117. https://doi.org/10.1016/j.ijhydene.2017.05.154.

[34] S. Tada, T. Shimizu, H. Kameyama, T. Haneda, R. Kikuchi, Ni/CeO_2 catalysts with high CO_2 methanation activity and high CH_4 selectivity at low temperatures, Int. J. Hydrogen Energy. 37 (2012) 5527–5531. https://doi.org/10.1016/j.ijhydene.2011.12.122.

[35] G. Zhou, H. Liu, K. Cui, A. Jia, G. Hu, Z. Jiao, Y. Liu, X. Zhang, Role of surface Ni and Ce species of Ni/CeO_2 catalyst in CO_2 methanation, Appl. Surf. Sci. 383 (2016) 248–252. https://doi.org/10.1016/j.apsusc.2016.04.180.

[36] Y. Hui, N. Ullah, L. Zhang, Z. Li, CO_2 methanation over nickel-based catalysts prepared by citric acid complexation method, Appl. Organometal. Chem. 34 (2020) 5268. https://doi.org/10.1002/aoc.5268.

[37] R.-P. Ye, Q. Li, W. Gong, T. Wang, J.J. Razink, L. Lin, Y.-Y. Qin, Z. Zhou, H. Adidharma, J. Tang, A.G. Russell, M. Fan, Y.-G. Yao, High-performance of nanostructured Ni/CeO_2 catalyst on CO_2 methanation, Appl. Catal. B Environ. (2019) 118474, Article in press. https://doi.org/10.1016/j.apcatb.2019.118474.

[38] A. Quindimil, U. De-La-Torre, B. Pereda-Ayo, A. Davó-Quiñonero, E. Bailón-García, D. Lozano-Castelló, J.A. González-Marcos, A. Bueno-López, J.R. González-Velasco, Effect of metal loading on the CO_2 methanation: A comparison between alumina supported Ni and Ru catalysts, Catal. Today. (2019) Article in press. https://doi.org/10.1016/j.cattod.2019.06.027.

[39] A. Cárdenas-Arenas, A. Quindimil, A. Davó-Quiñonero, E. Bailón-García, D. Lozano-Castelló, U. De-La-Torre, B. Pereda-Ayo, J.A. González-Marcos, J.R. González-Velasco, A. Bueno-López, Isotopic and *in situ* DRIFTS study of the CO_2 methanation mechanism using Ni/CeO_2 and Ni/Al_2O_3 catalysts, Appl. Catal. B Environ. 265 (2020) 118538. https://doi.org/10.1016/j.apcatb.2019.118538.

[40] J. Ashok, M.L. Ang, S. Kawi, Enhanced activity of CO_2 methanation over Ni/CeO_2-ZrO_2 catalysts: Influence of preparation methods, Catal. Today. 281 (2017) 304–311. https://doi.org/10.1016/j.cattod.2016.07.020.